Robotica (2004) volume 22, pp. 301–307. © 2004 Cambridge University Press
DOI: 10.1017/S0263574703005629 Printed in the United Kingdom

Robot positioning of flexible-link manipulator using vision

Halûk Küçük,* Gordon Parker† and Eric T. Baumgartner‡

(Received in Final Form: August 19, 2003)

SUMMARY
Vision-aided flexible link robot positoning using the Camera Space Manipulation (CSM) method is developed. The primary motivation for this work is to use an autonomous vision-aided robotic system to pick-up and accurately move a flexible object that it encounters. The work consists of analytical and experimental investigation of the performance of CSM for a kinematic model of the PUMA manipulator with a flexible structure at the wrist which accounts for the gravitation. Trade-offs between camera view parameters and axial deflection model parameters were investigated. View parameter reestimation and maneuvering resulted a very accurate placement of the end-effector at the target.

KEYWORDS: Machine vision; Camera space manipulation; Robot; Vision system.

1. INTRODUCTION

Flexible-link robot manipulation has been a very popular research in recent years where the applications mostly employed kinematics, deformation models, joint sensors or deformation sensors. Application of vision to flexible-link robot manipulation has been very limited.

One of the earliest applications of vision to flexible-link robot manipulation was proposed by Skaar *et al.*[1] Simulations have shown that the CSM method compensates for two particular kinds of errors: Unmodeled elastic deflection and unmodeled camera distortion. In their experiments Skaar *et al*. did not incorporate a large amount of elastic deflections as discussed in this paper. Accurately positioning of a flexible-link robot designed for International Space Station missions is simulated for pre-planned manipulations.[2] Nevertheless, task planning may not be possible for missions in unstructured environments. Tracking of deformable objects by using active deformable models, which attempts to minimize the object contour energy function including contour smoothness, continuity and local image contrast parameters, produced reliable results.[3] The performance of the energy method relies on the sufficient speed of minimization algorithms relative to the speed of the contour deformations in the image plane.

In remote environments of paramount importance are the robustness, computational efficiency in varying terrains and lighting conditions along with the limitations imposed by radiation hardened processor requirements and power constraints.[4] The amount of image information required for Camera Space Manipulation makes it a powerful method for unstructured environments. Also CSM provides a less computationally intensive vision-aided manipulation method, which is very important for any flexible manipulation where faster estimation is required to position the manipulator at the desired location. Much work has been accomplished in visual telerobotics, some using visual servoing and some alternative methods. Visual station keeping of indoor aerial blimps and remote operated underwater telerobots throughout monocular video sequence was accomplished by Van der Zwaan *et al*.[5] Conservation of the altitute of their underwater vehicle does not require the knowledge of proximity to the station, whereas in our problem, the manipulator end-effector has to guarantee convergence to the target. As a cost effective and safer approach compared to real-time visual servoing, a geometric, task space modelbased calibration of cameras was proposed by Kim.[6] His calibration architecture requires a 3-D virtual reality model of the real task environment for matching to the video images of the workspace. Hoffmann *et al*.[4] employed a method based on correlation of points-of interest on the right stereo image with their corresponding points in the left stereo image, and triangulation of the matched points using metrically calibrated camera models to determine their 3D position information. However, their triangulation routine requires metrically calibrated cameras.

An improvement of CSM is proposed in this paper; therefore, it is necessary to clearly describe its current state of the art. Selection of target in the image planes of the participating cameras and commanding the robot to minimize the error between the analytical and the sampled image plane coordinates is referred to as Camera Space Manipulation.[7] The method requires only image plane coordinate information, much less compared to visual servoing where the target is usually identified from a whole picture of the work environment. In CSM analytical mapping of the target onto the image plane is accomplished via camera view parameters estimated by sampling the end-effector image plane coordinates within the workspace. Minimization of the analytical model and the sampled image plane coordinates for the camera view parameters results in a set of view parameters valid for the workspace selected. Camera Space Manipulation usually utilizes a simplified version of a pin-hole camera model which assumes a constant to workplane distance. This assumption is valid for large camera to workspace distances compared to the movements of the manipulator within the workspace. The work presented in this paper consists of testing the performance

* Niğde University, Aksaray Faculty of Engineering, Aksaray (TURKEY). E-mail: hkucuk7@hotmail.com.
† Michigan Technological University (USA).
‡ Jet Propulsion Laboratory, California Institute of Technology (USA).

https://doi.org/10.1017/S0263574703005629 Published online by Cambridge University Press

of flexible-link CSM based on a kinematic model of the PUMA manipulator with a flexible payload carried at the wrist that accounts for the axial deformation. Furthermore, for end-effector positioning the conditions of existence of a set of camera view parameters under the presence of modeling errors were explored.

The paper is organized as follows: In Section 2, a mathematical model of the CSM method and view parameter estimation is presented. The theory of a flexible-link CSM is discussed in Section 3, where Puma kinematics with a flexible payload is explored. Camera view parameter estimation and CSM results are presented in Section 4. The paper is finalized by the discussion of the results in Section 5.

2. CAMERA SPACE MANIPULATION

As mentioned in the introduction, CSM is the method that will be used in this work for determining the robot configuration used to position the end-effector at a specified target. A brief review of the CSM method is given here only to the extent of introducing the relevant equations that will be used in later developments.

Camera Space Manipulation utilizes an orthographic camera model[8] to project Cartesian points onto image planes of participating cameras. The projection is represented by the following nonlinear equations.

$$\begin{aligned} x_c^i &= (C_1^{i^2}+C_2^{i^2}-C_3^{i^2}-C_4^{i^2})X+2(C_2^iC_3^i+C_1^iC_4^i)Y \\ &\quad +2(C_2^iC_4^i-C_1^iC_3^i)Z+C_5^i \\ y_c^i &= 2(C_2^iC_3^i-C_1^iC_4^i)X+(C_1^{i^2}-C_2^{i^2}+C_3^{i^2}-C_4^{i^2})Y \\ &\quad +2(C_3^iC_4^i-C_1^iC_2^i)Z+C_6^i \end{aligned} \tag{1}$$

where x_c^i and y_c^i are the coordinates of a target in the image plane of the ith camera, X, Y, Z are the elements of the Cartesian position vector and C_1^i, through C_6^i are the view parameters related to the Euler parameters.[7]

CSM requires experimentally determining values of $C_1^i,\cdots,C_6^i$ for each camera. This process is begun by sending the arm, with an attached target, along a predetermined path through the workspace of interest. At certain points along this path, the image plane coordinates of the target, denoted by (x_c^i, y_c^i) in each of the camera views is noted along with the corresponding joint configuration. It is assumed that the joint configuration data, denoted by $\underline{\theta}$ is supplied by sensors of the manipulator. The camera view parameters are then calculated from this data set using a numerical optimization code to find the values of the camera view parameters, $\underline{C}^i$ for the n participating cameras, that minimize the cost function

$$\Gamma_1 = \sum_{j=1}^{m}\sum_{i=1}^{n}\{(x_{c,j}^i - h_x[\underline{C}^i,\underline{P}_j(\underline{\theta})])^2+(y_{c,j}^i - h_y[\underline{C}^i,\underline{C}_j(\underline{\theta})])^2\} \tag{2}$$

where $x_{c,j}^i$ and $y_{c,j}^i$ are the image plane coordinates of the jth target as seen by the ith camera; $\underline{P}_j$ is the position of the jth cue as a robot end-effector known by $\underline{\theta}$ through forward kinematics of the arm; m is the number of cues used for the estimation process; h_x and h_y are the right hand side of Equation 1. After determining the view parameters, the CSM algorithm may be used to compute the robot's joint angles to achieve any cue specified by it's image plane coordinates (x_c^i,y_c^i), as seen by all n participating cameras by minimizing the cost function Γ_1.

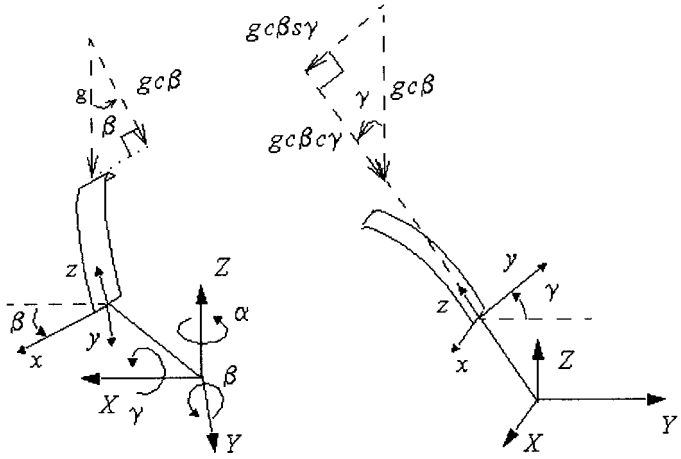


Fig. 1. Deflection of the flexible payload mounted on Puma.

3. FLEXIBLE-LINK CSM

Here PUMA kinematics with a flexible payload was developed. Different transverse and axial models are discussed. The robot employed here is PUMA 700 industrial purpose robot. It has 6 degrees of freedom.[9] A flexible sheet beam was mounted at the wrist joint such that the x-z plane was tangent to the flat surface. The deflection in the x-direction and torsion was assumed to be negligibly small [Figure 1]. The component of gravitational force along y and z-axis govern deflections of the flexible link along those directions.

The wrist joint of the robot is fixed for simplification purposes as $\theta_4=\theta_5=0$, and $\theta_6=90°$. The details of this assumption will be explained later in the section. General rotation matrix representing the orientation of the end-effector with respect to the base frame can be written both in terms of robot joint angles and flexible-link orientation angles (γ, β, α) [Figure 1], based on $X-Y-Z$ fixed angles convention.[9] Equating these two different rotation matrices and solving for rotation angles (γ, β, α) results,

$$\begin{aligned} \beta &= \tan^{-1}(-r_{31},\sqrt{r_{11}^2+r_{21}^2}) \\ \alpha &= \tan^{-1}(r_{21}/c_\beta, r_{11}/c_\beta) \\ \gamma &= \tan^{-1}(r_{32}.c_\beta, r_{33}/c_\beta) \end{aligned} \tag{3}$$

where r_{ij} are components of the rotation matrix written in terms of robot joint angles. Gravity can be decomposed into transverse (y-direction) and axial (z-direction) components as shown in Figure 1. Since deflection is a function of gravity and orientation, transverse deflection can be modeled as

$$\delta = \delta_{\max} c_\beta s_\gamma \tag{4}$$

where $\delta_{\max}$ is maximum transverse deflection.

In the optimization, a maximum transverse deflection is introduced as an estimation parameter Q_1, and the deflection depicted in Equation 4 is modeled as

$$\delta = Q_1 c_\beta s_\gamma \tag{5}$$

The axial deflection of the beam can be modeled as a linear estimation parameter,

https://doi.org/10.1017/S0263574703005629 Published online by Cambridge University Press

$$\Delta = Q_2 \tag{6}$$

Similar to transverse deflection, axial deflection can be modeled as

$$\Delta = Q_2 c_\beta c_\gamma \tag{7}$$

where Q_2 is an optimization parameter which replaces maximum axial deflection and the $c_\beta c_v$ term decomposes the gravity into its axial component.

Large deformations of cantilever beams, that are subject to distributed loadings can be solved by using pseudolinear equivalent systems. The beam deflecting by its own weight can be considered as a uniform flexible beam loaded with uniformly distributed weight w. Fertis[10] provided an approximate solution of axial deflection for distributed loaded beams. The axial displacement Δ can be determined by solving

$$L = \int_0^{L-\Delta} \{1 + y'^2\}^{1/2} dx \tag{8}$$

where

$$y'(x) = \frac{f(x)}{\{[1 - f(x)]^2\}^{1/2}}$$

and

$$f(x) = -\frac{w}{12EI}[2x^3 + 3\Delta x^2 + (L-\Delta)^3 - 3L(L-\Delta)^2].$$

Here L is the beam length and EI is the material stiffness. Approximate expressions for the variation of $\Delta(x)$ can be used and Fertis have proven to provide accurate results for different $\Delta(x)$ approximations. For a 1654 mm long 19.05 mm wide and 3.175 mm thick horizontally oriented *Al* beam maximum deflection was measured to be 55.3 mm. The nonlinear model, prediction of axial deflection for alternative $\Delta(x)$ approximations are listed in Table I. The nonlinear scheme employed here utilizes a deformation model which define the deflection as a function of the horizontal position, the $\Delta(x) = \Delta\sqrt{x/L_O}$ where $0 \le x \le L_O$ and $L_O = L - \Delta$. Although the constant deformation model demonstrates the least error overall, considering arbitrary boundary conditions by utilizing a horizontal-position dependent deflection function would be appropriate.

Inverse kinematics solution to flexible body kinematics yields infinite number of joint configuration solutions. To be able to demonstrate this, a flexible link can be oriented ε and φ degrees about X and Y axis respectively such that the tip lies at a fixed point A [Figure 2]. We need to prove that there are infinite number of $\varepsilon - \varphi$ combinations to satisfy this condition.

Table I. Maximum axial deformations and corresponding errors for different deformation functions.

deflection function	deflection Δ (mm)	error (%)
$\Delta(x) = \Delta$	1.22	2.21
$\Delta(x) = \Delta(x/L_O)$	6.26	11.32
$\Delta(x) = \Delta\sqrt{x.L_O}$	4.51	8.15
$\Delta(x) = \Delta\sin(\pi x/2L_O)$	4.92	8.90

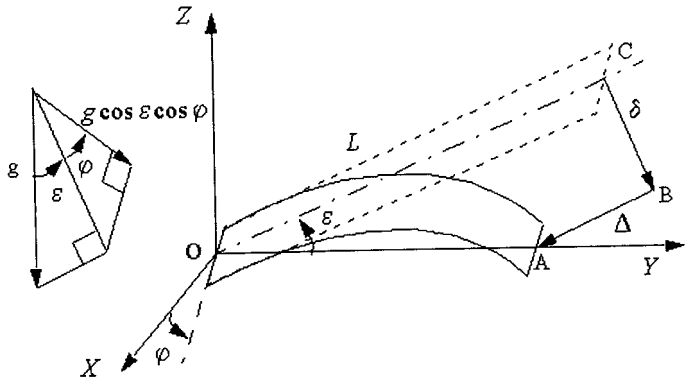


Fig. 2. Transverse and axial deflection of the beam, subject to its own weight.

Here δ and Δ represent transverse and axial deflections respectively. L is the original length of the beam. The component of gravity normal to the flat surface of the beam is $g \cos \varepsilon \cos \varphi$.

One can write the following vectorial equation for the polygon OABC.

$$O\bar{C} = O\bar{A} + A\bar{B} + B\bar{C} \tag{9}$$

Using complex mathematics and solving the above equation for $O\bar{A}$, results

$$O\bar{A} = Le^{i\varepsilon} - \Delta e^{i\varepsilon} - i\delta e^{i\varepsilon} \tag{10}$$

From classical mechanics, transverse deflection can be written as $\delta = wL^4/8EI$, where w is mass per length, L is the length of the beam, E is Young's modulus and I is moment of inertia. Due to orientation of the flexible beam transverse deflection becomes $\delta = w\cos\varepsilon\cos\varphi L^4/8EI$. Now for known ε, Equation 8 and Equation 10 can be solved simultaneously to determine Δ and φ subject to the constraint $REAL(O\bar{A}) = |O\bar{A}|$ and $IMAG(O\bar{A}) = 0$ which satisfies the requirement that the tip lies at point A. Solution of Equation 8 and Equation 10 for a 1654 mm long 19.05 mm wide and 3.175 mm thick horizontally oriented *Al* is depicted in Figure 3.

One can expect, if φ is fixed then there exists a single solution to the flexible-link inverse kinematics problem. To be able to compensate for this phenomenon, the wrist angles of PUMA were fixed as $\theta_4 = \theta_5 = 0$, and $\theta_6 = 90°$.

Now the improved cost function for flexible-payload CSM takes the form

$$\Gamma_2 = \sum_{j=1}^{m} \sum_{i=1}^{n} \{(x_{c,j}^i - h_x[\underline{C}^i, \underline{P}_j(\underline{\theta}, \delta, \Delta)])^2 + (y_{c,j}^i - h_y[\underline{C}^i, \underline{P}_j(\underline{\theta}, \delta, \Delta)])^2\} \tag{11}$$

where δ and Δ depict transverse and axial deflections, respectively, whose associated parameters need to be determined along with the camera view parameters $\underline{C}^i$.

https://doi.org/10.1017/S0263574703005629 Published online by Cambridge University Press

4. EXPERIMENTAL SETUP AND A PROCEDURE

Flexible CSM was experimented on a PUMA 700 model robot. A lm long, 0.1m wide and lmm thick, thin sheet aluminum beam was mounted at the wrist of the robot. Two colored balls were used as end effector and target for visibility purposes. End effector and target were represented with a blue ball attached to the tip of the flexible payload and a yellow ball hanging from the ceiling, respectively. The experiments were carried out for different flexible kinematics approaches. The performance of different models were discussed in terms of mapping from 3-D space onto image plane and end effector positioning accuracy.

4.1. Estimation Results for Manipulator With a Flexible-Payload

The view parameter estimation for the Puma robot is accomplished by moving the robot through 22 different joint configurations and sampling the corresponding end effector image plane coordinates. The reader is referred to Küçük[11] for relevant data. The estimation is accomplished by employing the transverse deflection model depicted in Equation 5. For axial deflection, various models are utilized as in: (a) Equation 6, (b) Equation 7 and (c) Equation 8 and camera view parameters and associated optimization cost are listed in Table II and Table III, respectively. No end-effector orientation requirement was imposed for this positioning task.

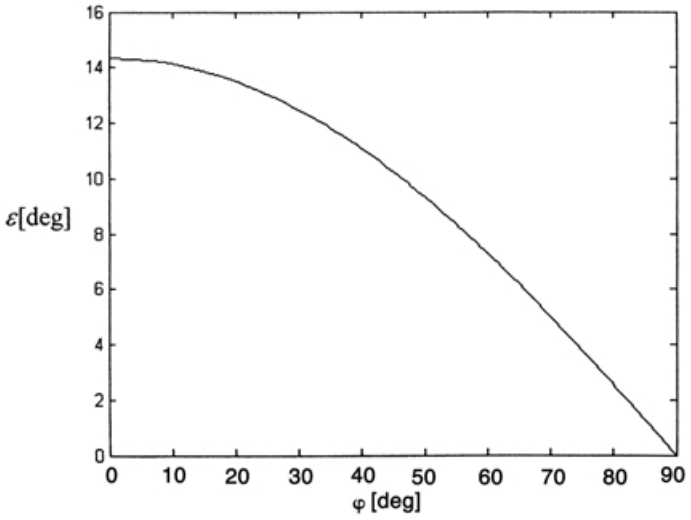


Fig. 3. Inverse kinematics solution of a flexible link.

As seen from Table III, Equation 8 demonstrates the least optimization cost. The model depicted by this equation compensates for nonlinear deflection characteristics better than the linear mechanics solution.

(a) Linear axial deflection model:. Initially, transverse and axial tip deflections were modeled as in Equation 5 and Equation 6, respectively. Flexible-link parameters were optimized to be $Q_1 = -933650$ and $Q_2 = -1042665$. After completion of the estimation, the mapping of 22 sample data points onto the image plane, was performed with calibrated parameters. A maximum pixel error between the analytical and real image plane coordinates was observed to be 65 pixels.

(b) Nonlinear axial deflection model:. Transverse and axial tip deflections were modeled as in Equation 5 and Equation 7, respectively. Flexible-link parameters were estimated to be $Q_1 = -1257684$ and $Q_2 = -1383799$. The mapping of joint space onto image plane was accomplished via estimation parameters provided by a nonlinear flexible body kinematics model. Maximum pixel error was observed to be 16 pixels.

Table II. Optimal camera view parameters for various models.

View parameters	Model a Equation (5) and Equation (6)		Model b Equation (5) and Equation (7)		Model a Equation (5) and Equation (8)	
C_j^i	Camera #1 (i=1)	Camera #2 (i=2)	Camera #1 (i=1)	Camera #2 (i=2)	Camera #1 (i=1)	Camera #2 (i=2)
C_1^i	−0.0143	−0.0193	0.1780	0.2533	−0.1786	−0.2527
C_2^i	−0.0096	−0.0172	−0.1449	−0.2266	0.1482	0.2270
C_3^i	−0.0133	−0.0067	−0.2218	−0.1441	0.2227	0.1481
C_4^i	−0.0183	−0.0105	0.2739	0.1695	−0.2750	−0.1708
C_5^i	355.2554	220.3222	329.1380	388.8518	325.9581	335.0397
C_6^i	−663.9886	−662.3913	2769.0866	2677.0080	400.3275	436.5871

Table III. View parameter optimization and CSM results for different axial models.

axial model	optimization cost Γ_2 (pixel^2)	optimum joint angles $(\theta_1 \cdots \theta_3)^*$ [deg]	CSM cost Γ_2 (pixel^2)
Equation (6)	52302.0	[105.8, −210.0, −119.0]	18.6253
Equation (7)	4039.6	[105.7, −200.2, −133.9]	0.2019
Equation (8)	3686.3	[105.9, −200.0, −132.2]	0.0559

https://doi.org/10.1017/S0263574703005629 Published online by Cambridge University Press

(c) Nonlinear mechanics deflection model:. Transverse and axial tip deflections were modeled as in Equation 5 and Equation 8, respectively. The nonlinear scheme employed here utilizes a deformation model which define the axial deflection as a function of horizontal position, the $\Delta(x)=\Delta\sqrt{x/L_O}$ where $0\leq x\leq L_O$ and $L_O=L-\Delta$. Since, the axial deflection is estimated based on the nonlinear mechanics model there is no estimation of Q_2 parameter for this case. The flexible beam parameter for transverse deflection was optimized to be $Q_1=1103.56$. The mapping of joint space onto image plane was accomplished with view parameters provided by a nonlinear flexible payload kinematics model. A maximum pixel error was observed to be 14 pixels.

4.2. CSM Results for Manipulator With a Flexible Payload

After view parameter estimation, the robot was oriented in a configuration and the joint angles were recorded through the software of the robot. The joint configuration of the robot was $[\theta_1 \cdots \theta_3]=[106\ \ -169\ \ -147]$ degrees. After positioning the robot at this configuration the image plane coordinates of the end-effector were recorded as $[x_c^1\ y_c^1\ x_c^2\ y_c^2]=[426\ 209\ 394\ 264]$ pixels. The robot was moved away from this configuration to $[\theta_1 \cdots \theta_3]=[50\ -180\ -180]$ and the CSM code was executed to position the robot at the target. Camera Space Manipulation for different flexible payload kinematics model results are listed in Table III. As seen from the table, Equation 8 yields a very good positioning accuracy whereas linear axial deflection model approximation does not provide an accurate positioning accuracy. However, the amount of computation required by Equation 8 is excessive. Hence, further experimentation of flexible CSM, was performed by using the axial deflection model described by Equation 7. First, the robot was positioned in a certain configuration and image plane coordinates of the end-effector along with the associated joint angles were sampled, The robot was moved away from the sampled configuration and CSM was performed based on the image plane information. The results are presented in Table IV, maximum image plane error was observed with task No. 5 and a minimum error was observed with task No. 4.

Multi-step CSM:. Camera Space Manipulation requires one to re-estimate camera view parameters as the manipulators is moved along the path from the initial position to the target. The re-estimation of camera view parameters is accomplished by sampling the image plane coordinates and associated joint configuration of the robot at intermediate steps. Best case scenarios may result in a one step CSM for an end-effector to target a positioning task. Introducing a link length error into the kinematics of the robot may result in a positioning error with the end-effector, which may force a multi-step CSM. The advantage of having a multi-step CSM is a contraction of the camera view parameter space around the target, thus resulting in a view parameter set, which may position the end-effector with better accuracy.

In order to accomplish CSM parameter re-localization, a 100% link length error was introduced into the kinematics by multiplying the actual length of the flexible link. The robot was positioned at $[\theta_1 \cdots \theta_3]=[-115,\ -160,\ -150]$ degrees orientation where the image plane coordinates of the end-effector were recorded as $[x_c^1\ y_c^1\ x_c^2\ y_c^2]=[241\ 198\ 219\ 226]$ pixels. The target was chosen as $[x_c^1\ y_c^1\ x_c^2\ y_c^2]=[525\ 251\ 467\ 311]$ pixels. After initial parameter estimation, the CSM code was executed to position the end-effector at the target. At each step, the outermost and innermost distances between the end-effector and target balls were measured [Table V]. The first CSM step resulted a positioning error of 9.25 cm which is the average of outermost and innermost distances. After 4 iterations positioning of the end-effector at the target was accomplished with reasonable accuracy [Table V].

Table IV. CSM results for different positioning tasks.

Test	joint space, $(\theta_1 \cdots \theta_3)$ [deg]		camera sace, $[x_c^1, y_c^1, x_c^2, y_c^2]$ (pix)		
No.	starting angles	optimum angles	target position	final position	error
1	[100, −170, −140]	[105.7, −163.3, −146.8]	[541, 292, 486, 343]	[541, 278, 479, 332]	0, 14, 7, 11]
2	[125, −150, −145]	[121.8, −161.1, −142.7]	[551, 350, 447, 389]	[536, 319, 444, 364]	[15, 31, 3, 25]
3	[80, −175, −165]	[72.0, −169.6, −168.2]	[389, 125, 396, 187]	[404, 118, 414, 187]	[−15, 7, −18, 0]
4	[−120, −165, −155]	[−118.7, −176.8, −147.1]	[212, 247, 185, 268]	[219, 248, 201, 273]	[−7, −1, −16, −5]
5	[−115, −145, −140]	[−118.7, −154.8, −141.2]	[158, 410, 106, 429]	[178, 368, 125, 385]	[−20, 42, −19, 44]

Table V. Multiple CSM results.

step No.	joint angles $(\theta_1 \cdots \theta_3)$ [deg]	image coordinates $[x_c^1, y_c^1, x_c^2, y_c^2]$ (pix)	outermost, innermost distance (cm)
1	[106.75, −176.17, −140.24]	[515, 270, 460, 323]	13, 5.5
2	[106.58, −172.33, −143.7]	[518, 216, 461, 318]	9.5, 2.5
3	[106.37, −170.08, −145.7]	[519, 258, 462, 314]	7.75, 0.75
4	[106.28, −169.08, −146.57]	[519, 257, 463, 314]	7, 0

https://doi.org/10.1017/S0263574703005629 Published online by Cambridge University Press

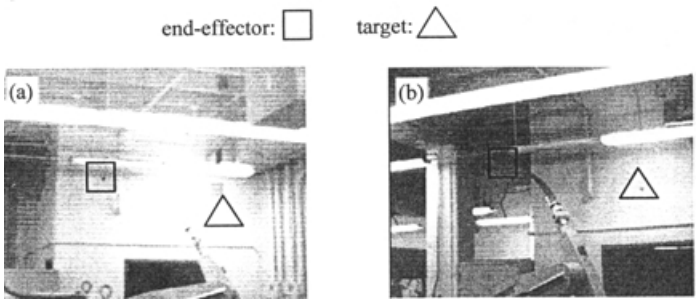


Fig. 4. Initial orientation. (a) Camera 1; (b) Camera 2.

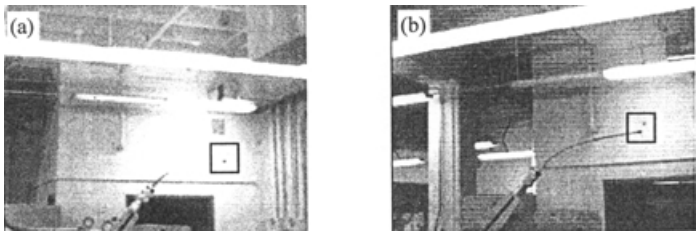


Fig. 5. Iteration No. 1.

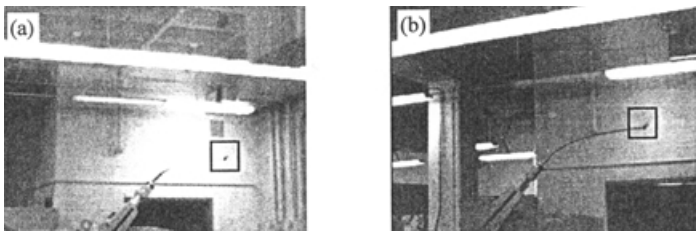


Fig. 6. Interation No. 4.

The multi-step CSM in view of the two participating cameras is shown in Figures 4, 5 and 6. The re-estimation of the camera view parameters is one of the most important phases of CSM. In practical applications, target identification is done by machine vision techniques. No operator is involved.

5. CONCLUSIONS

A new method for flexible link positioning using Camera Space Manipulation was developed. The method developed for flexible beam kinematics accounts for the gravitation. Examination of the method was performed on a PUMA 700 robot with a lm long, 0.1 m wide and lmm thick thin sheet aluminum beam attached to the wrist. The maximum deflection of the beam, which occurs at horizontal orientation, is scaled based on the orientation of the beam for both axial and transverse deflections. For large deformations, Fertis[10] used a nonlinear model which is based on the assumption that length of the deformed beam is equivalent to its original length. Both the proposed axial deflection model and nonlinear mechanics model approach were experimented. The PUMA robot was moved within the workspace and 22 orientations and corresponding end-effector image plane coordinates were selected for carnera view parameter estimation. The manipulator was moved to a known orientation and the image plane coordinates were selected for Camera Space Manipulation. Then the manipulator was moved to an arbitrary orientation and CSM code was commanded with the sampled image coordinates. The proposed model demonstrated a very close performance to the nonlinear mechanics model approach.

Camera view parameters provide a mapping of the sample points onto the image plane. In order to improve the mapping, thus end-effector placement accuracy, a re-estimation of the camera view parameters as the manipulator moves closer to the target, is crucial. In order to investigate this phenomena, a blue ball of foam was attached to the end-effector of the flexible beam and a yellow ball of foam was hanged form the ceiling, as a target. To guarantee a requirement for re-estimation, a 100% link length error is introduced by multiplying the actual length of the flexible link. This, relaxed the camera view parameter estimation cost and resulted in an error with the end-effector placement. Camera view parameters were re-estimated after the first iteration. Four, consecutive reestimation and maneuvering resulted a very accurate placement of the end-effector at the target.

Scaling of the maximum axial deflection based on the orientation results in a compatible placement strategy. Contraction of the estimation around the target by reestimation of the camera view parameters, guarantee the convergence of the end-effector to target.

In contrast to visual servoing employed by Stieber *et al.*[2] and most of the researchers, CSM provides a less computational intensive method which is imperative for flexible manipulation. Also, the amount of image information required for CSM, makes it a powerful method for unstructured environments.

Acknowledgements

This work was supported in part by NSF under contract NSF-9622669 and by the MTU College of Engineering.

References

1. S. B. Skaar, W. H. Brockman and W. S. Jang, "Three-dimensional camera-space manipulation", *Int. J. Robot. Res.* **9**, 22–39 (1990).
2. M. E. Stieber, M. McKay, G. Vukovich and E. Petriu, "Vision-based sensing and control for space robotics applications", *IEEE Transactions on Instrumentation and Measurements* **48**, 807–812 (1999).
3. M. J. Sullivan and N. P. Papanikolopoulos, "Using active deformable models to track deformable objects in robotic visual servoing experiments", *Proceedings of the IEEE International Conference on Robotics and Automation* (1996), **Vol. 4**, pp. 2929–2934.
4. B. D. Hoffman, E. T. Baumgartner, T. L. Huntsberger and P. S. Schenker, "Improved rover state estimation in challenging terrain", *Autonomous Robots* **6**, 113–130 (1999).
5. S. Van der Zwaan, A. Bernardino, J. Santos-Victor, "Visual station keeping for floationg robots in unstructured environments", *Robotics and Autonomous Systems* **39**, 145–155 (2002).
6. W. S. Kim, "Computer vision assisted virtual reality calibration", *IEEE Transactions on Robotics and Automation* **5**, 450–464 (1999).
7. S. B. Skaar, W. H. Brockman and R. Hanson, "Camera space manipulation", *Int. J. Robot. Res.* **6**, 22–39 (1987).

https://doi.org/10.1017/S0263574703005629 Published online by Cambridge University Press

8. G. Hager, S. Hutchinson and P. Corke, "A tutorial introduction to visual servo control", *IEEE Transactions on Robotics and Automation* **12**, 651–670 (1996).
9. J. J. Craig, *Introduction to Robotics-Mechanics and Control* (2nd Edition, Addison-Wesley Publishing Company, 1989).
10. D. G. Fertis, *Nonlinear Mechanics* (CRC Press, 1993).
11. H. Küçük, "Vision-based path planning for flexible-link robotics", *Ph.D. Thesis* (Department of Mechanical Engineering-Engineering Mechanics, Michigan Technological University, MI, 1999).

https://doi.org/10.1017/S0263574703005629 Published online by Cambridge University Press